# Sorting microplastics from other materials in water samples by ultra-high-definition imaging

Kai-Erik Peiponen[1], Boniphace Kanyathare[1], Blaž Hrovat[2], Nikolaos Papamatthaiakis[3], Joni Hattuniemi[4], Benjamin Asamoah[1], Antti Haapala[3,5], Arto Koistinen[2], and Matthieu Roussey[1]

[1] Department of Physics and Mathematics, Center for Photonics Sciences, University of Eastern Finland, P.O. Box 111, 80101 Joensuu, Finland.

[2] Department of Technical Physics, University of Eastern Finland, P.O. Box 1627, 70211 Kuopio, Finland.

[3] School of Forest Sciences, University of Eastern Finland, PO Box 111, 80101 Joensuu, Finland.

[4] Valmet Automation Inc., Kehräämöntie 3, 87400 Kajaani, Finland.

[5] FSCN Research Centre, Mid Sweden University, SE-85170 Sundsvall, Sweden.

## Abstract

In this study a commercial particle analyzer was used to image and help sorting microplastic particles (MPs) dispersed in filtrated and de-aerated tap water. The device provides a relatively easy and fast procedure for obtaining ultra-high-definition imaging, allowing the determination of shape, size, and number of 2D-projections of solid particles. The image analysis revealed clear differences among the studied different MPs originating from the grinding of five common grades of plastic sheets as they affect the image rendering differently, principally due to the light scattering either at the surface or in the volume of the microplastics. The high-quality imaging of the device also allows the discrimination of the microplastics from air bubbles with well-defined spherical shapes as well as to obtain an estimate of the size of MPs in a snapshot. We associate the differences among the shapes of the identified MPs in this study depending on the plastic type with known physical properties, such as brittleness, crystallinity, or softness. Furthermore, as a novel method we exploit a parameter based on the light intensity map from moving particles in cuvette flow to sort MPs from other particles, such as, wood fiber, human hair, and air bubbles. Using the light intensity map, which is related to the plastic-water refractive index ratio, the presence of microplastics in water can be revealed among other particles, but not their specific plastic type.

## 1. Introduction

Microplastics (MP) in open water is currently a global problem affecting health, environment, and economy [1-3]. The main obstacle to a solution to counter the spread of MPs is the lack of appropriate




This provisional PDF is the accepted version. The article should be cited as: J. Eur. Opt. Society-Rapid Publ., https://doi.org/10.1051/jeos/2023010

devices to detect these particles in aquatic environment and in situ. The main reason comes from the fact that MPs undergo different interactions with the environment. The complex shape and small size of MPs makes their properties different from pristine ones, which leads to an inappropriateness of the international standards for the definition of quality of macroscopic plastic products. A current limitation on the identification and analysis of MPs is the need for sample preparation, which is also required for some spectral measurement techniques, such as Fourier-transform infrared (FTIR) and Raman spectroscopy [4-6]. Currently, emerging method to detect MPs utilize hyperspectral imaging of dry MPs [7]. However, other methods such as digital holographic microscopy [8,9], laser speckle pattern [10] and smartphone-enabled method [11] requiring neither sample treatment nor sorting have shown promises for MP detection directly from water. Nevertheless, the water volume probed at once by these devices remains rather small and not convenient for large field study. Similarly, other flow field applications for microparticles such as flow cytometer [12,13] are impaired in the use of unfiltered samples due to strict limitations in the flow cavity dimensions that are prone to blockages in case the sample has a wide particle size distribution or even a few particles beyond or close to the flow tube dimensions. There is an inevitable need for devices with larger volume for MP detection in water and real-time and in situ applications.

Besides the shape and size, another factor contributing to the challenges in MP detection in water is their appearance. Plastics can be transparent or hazy in water [14] and, by extension, MPs can exhibit similar characteristics. Haziness from plastics can be due to surface roughening of originally transparent (clear) plastic by mechanical wear, by chemical reaction, or due to refractive index inhomogeneity in the volume of the plastic originating from external stress. In all cases, light is scattered from the plastic, which causes translucent or opaque appearance of the sample. Both transparency (ISO 13468-2, ASTM D1746-09) and haziness (ISO 14782: 2021 (en), ASTM D1003-21) of plastics are commonly detected using a spectrophotometer. Information on ageing of transparent or white plastic caused by an exposure to Sun light, moisture, temperature, and chemical reactions, is also obtained by the so-called yellowness index (YI, ISO 17234:2014), which is extracted from the spectrum of the plastic sample in the visible range of light. The concept of yellowness index has been exploited, e.g., in the investigation of marine pellets [15].

However, the above figures of merit are based on optical measurements of plastics in air. In principle, similar definitions and standards of plastic quality as above can be extended to describe macroscopic plastics or MPs in aquatic environments, but the probed area of the sample has to be flat and there is the issue of water absorption especially in the spectral region of near-infrared radiation. Measurement conditions can be much more complex in real water systems, e.g., open, industrial, or waste waters,

than in laboratory-prepared samples due to the presence of other organic and inorganic materials than plastics, and MPs having irregular and non-flat structures. Finally, temporal changes in the measurement conditions and the lack of suitable measurement devices can often make difficult the interpretation of the results.

Subjective visual inspection [16-18] has been one of the methods considered for the identifications of MPs, despite a reduced reliability of MP detection due to possible human interference. Moreover, for smaller MP sizes, in micron range, visual inspection becomes challenging [19,16]. Therefore, we suggest, in this paper, the use of an imaging device, primarily developed for wood fibers and fines analysis [20], as a promising tool to read various properties of MPs from a water sample volume without sample pretreatment other than diluting microplastics containing water sample by tap water. Using a novel concept of light intensity bitmap in the field of MP studies, it is possible to distinguish unknown particles from other unknown inorganic or organic particles, that are simultaneously present in the water sample to belong to the material group of plastics. The light intensity bitmap depends on the refractive index ratio between plastics and water and depends on the wavelength of visible light [21]. We demonstrate the viability of light intensity bitmap using homemade MPs in a water volume. We note that other microscope-based techniques, such as binocular dissecting microscopes [22] and near-infrared hyperspectral imaging [23], are alternative MP identification solutions, although they are usually used on dry samples after pretreatment of samples [24].

## 2. Materials and Methods

The plastic samples used for the preparation of the artificial MPs are commercial sheets from Goodfellow Ltd (UK). Studied MP samples include low-density polyethylene (LDPE), polystyrene (PS), polypropylene (PP), polyamide (PA) and unplasticized polyvinyl chloride (UPVC). The MPs were obtained by grinding plastic pieces with Retsch Ultra Centrifugal Mill ZM 200. Before grinding, the plastic sheets were cut into small pieces under 1 $cm^2$ and hardened in liquid nitrogen for an easier grinding. These pieces were then inserted into the mill in small amounts together with a spoonful of liquid nitrogen to prevent the plastic from melting during grinding. Sieves with 1 mm- and 0.25 mm-mesh sizes were used in sieving the resulting MPs during the grinding. The grinding speed was 10,000 rpm in the case of the 1 mm sieve and 6,000 rpm in the case of the 0.25 mm sieve, to avoid overheating of the plastics. The grinding yields nano- and microplastics in the size range 100 nm- 250 µm and these have different morphologies, which was confirmed by SEM analysis.

Valmet Fiber Image Analyzer (Valmet FS5) is an offline fiber and particle image analyzer for daily laboratory or research use. Equipped, in this version, with an Ultra-High-Definition imaging unit (UHD), it can be used for very tiny particle detection such as MPs. It was developed primarily for fiber and particle analyses in pulp and paper industry. The device consists mainly of a sample handling unit, an imaging unit and a touch screen user interface unit, all connected via computer. The sample is diluted in tap water and is being pumped through the sample circulation loop. Consistency of the sample can be set by hand or let the device adjust the consistency to the value set by user. The sample flows through a flow cell in which particles are being illuminated and imaged with industrial area scan monochrome camera. Imaging area is broad enough to measure large (10 mm) particles and accurate for the observation of the smaller ones (minimum detectable particle dimension is in the range of 1 µm). We exploit in this study snapshot images but it is also possible to record video from the moving objects, e.g., MPs, and observe their changing appearance as a function of time as the water flow propagates. Such a method is not the focus of this article; however, similar to stereomicroscopic view, it would lead to three-dimensional representation of the objects within the water sample and yield a better description of the immersed objects. The measurement of one 0.5 L sample, volume chosen for this study, is based on the circulation measurement mode of the device and it takes about 4 min depending on the sample type and settings chosen by the user. There is also the option of non-circulation measurement. In such a case the sample volume (in principle infinite) is not limited but it goes to waste. We preferred the circulation mode to preserve the MPs for future use. One measurement typically can include hundreds of thousands of particles. In the case there were only a single MP, of a size from 1 µm or larger in the water sample, it would be detected by the imaging device once it passes the detection window. As a proof of concept each plastic type was analyzed separately. The software calculates the morphological properties of the objects. Particle length, width, area, and count are the most common properties reported by the device. In our case, the analysis is done partly independently on the device's software since it must be taught beforehand to recognize the different particle/object types. This could be realized with machine learning that has been suggested, e.g., to automize data handling in holographic imaging of MPs [25]. Yet, machine learning is efficient also in such a case to monitor, e.g., 3D structures of transparent microscopic objects [26] but would require some changes in the case of the detection setup to obtain interesting 3D appearance of transparent MPs. Note that the method described by Horisaki et al. can be used also for opaque objects by detecting reflected light from an object.

The light intensity distribution of the imaged objects is obtained as a bitmap that is used in further analysis of the MPs, as a novel method to screen MPs from other objects in flowing water. We

developed an additional analysis method enabling a better rendering of the captured images and an improved contrast. This methodology described together with the results, for better clarity, is based on the calculation of a spatial intensity quantity, M, defined as $\mathrm{M} = \frac{I(x,y)}{I_0(x,y)}$. In this equation, $I(x,y)$ is the intensity of the $(x,y)$ pixel of one image and $I_0(x,y)$ the intensity at the same image pixel of a reference (background) image, captured with no particle inside the measuring chamber. The illumination and imaging system of the used device is certified to be highly stable, which allow us this data processing. By definition, $0 \leq \mathrm{M} \leq 1$. However, M may be greater than 1, depending on the chemical structure of the particle and its inherent optical properties. Later, results are presented as 1 – M, for an even better visibility of the particles. The light intensity bitmap M depends on the refractive index of the object and ambient medium, such as water. Wavelength-dependent refractive index of a medium is an intrinsic material property that can be used for the identification of the object similar to spectral fingerprints of a medium. Artificial MPs tend to have a rather homogenous spatial refractive index, and hence this property can be used for sorting them from other particles in water.

## 3. Results

The pristine plastic samples of this study are transparent or translucent in air. Scattering of light from such plastics immersed in water is much weaker than in the air. The scattering of light is strongest when the size of the scatterer or its features, such as the surface roughness, is of the same order as magnitude as the wavelength of the incident light. However, it is important to distinguish between surface and volume scattering of an MP. While MP is embedded in water, the scattering from surface roughness can be weak when the average surface roughness of MP is smaller than the effective wavelength (in water) of the probing light. The strength of light scattering also depends on the magnitude of the refractive index difference between the plastic sample and the ambient water. The smaller the refractive index difference, the weaker the surface scattering resulting from microroughness. In the case of volume scattering, due to volume inhomogeneities inside the MP, the situation is different because water is not in contact with the internal parts of the MP. Therefore, volume scattering is an intrinsic property of a particular MP. However, if the plastic is porous, then water can penetrate the pores and hence influence the strength of volume scattering of light. Ageing of plastic and the mechanical stress such as induced by our fabrication method, can affect both the extrinsic and intrinsic properties of plastics, e.g., light scattering, which can similarly influence the optical properties of the MPs.

We first deal with irregular sizes and shapes of MPs detected by the imaging tool and related peculiar optical properties, such as, a lens formation or hole inside a MP. Figure 1 shows images of MPs in water obtained for different types of MP. Figure 1a is an example of image obtained for PA MPs. These MPs appear as dark and irregular contrary to observations in classical bright-field imaging. In typical bright-field microscopy, transparent objects usually have low image contrast with its background. Here, on the contrary, one can observe that the MPs, within this size range, show high image contrast. This is certainly due to light scattering since PA is translucent, as stated above.

It is to be noted, in Fig. 1a, that many well-defined circular objects of various sizes are also present. These are air bubbles formed by the stirring of water in the volume compartment with a propeller. The biggest one is about 1.87 mm in diameter, while some smaller ones have diameters of 225 µm or 60 µm. The air bubbles appear dark because light is incident from denser medium, i.e., water (refractive index, RI: $n$ = 1.33), to air ($n$ = 1) and the light rays can experience reflection at the boundary, refraction across the boundaries, or total reflection. Additionally, the observed darkness of the air bubbles can also be explained using the refractive index difference between the various constituents. For example, the RI difference between water and air is larger than of the one between water and the MPs. The theory of the influence of the RI difference on the appearance of the air bubbles (dark), their radius-dependent optical properties, and other experiments on air bubbles in water are explained in [27]. In principle, air bubbles can be used as reference particles with well-known optical properties. Similar air bubbles can also be identified in the other studied images. More detailed studies on the behavior of air bubbles in water can be found for instance in these two articles [28,29].

The device's software has already an algorithm to neglect the air bubbles in the counting of the identified particles in the analysis of an image. Note that this function was disabled for this current study. In the practical case of MP imaging, omitting air bubbles simplifies the monitoring of particles and their abundance in a water sample. It is also possible that a MP acts as a nucleation unit of air bubbles. An example of it is shown in Fig. 1e, where several bubbles (half spheres) are on a smooth (average surface roughness (measured with Mitutoyo SJ-210 profilometer, Japan) on both sides ca. 0.06 µm) hand-cut MP-film type of PET. As a side remark, bubbles can affect strongly the conclusions drawn after optical detection of hydrophobic MPs by modifying the lift of the particles. This may yield a confusion between a low- or high-density plastic if the air bubbles are not identified. Since the setup uses a vertical flow it has practical importance regarding monitoring of air bubble attachment on MPs, a method that has been suggested for the enrichment of microplastics in vertical water flow [30]. We remark that according to the theory of optics, primary spherical MPs will yield

192 different light intensity bitmap from air bubbles because the refractive index contrast of water-air
193 bubble interface is much higher than that of water-primary MP interface, and there is no total
194 reflection present in the case of water-primary MP.

195 In Fig. 1b, several fragments of PP can be observed (circled in green and brown), which also appears
196 as a dark pattern due to light scattering like the other samples. Fig. 1c shows identified fragments of
197 LDPE. The larger fragment (highlighted in a red rectangle) is rather irregular, and a quantity such as
198 "aspect ratio" has little meaning in this case. Fig. 1d shows a zoomed-in image of the bigger LDPE
199 fragment. The interesting feature in the enlarged image is that, in the false color presentation of the
200 light intensity distribution, one can distinguish both dark (blueish) and bright (yellowish) locations in
201 the MP area. Very bright patterns correspond to transparent locations. After a detailed analysis of the
202 bitmap intensity of this MP, it turned out that some of the bright spots are much brighter than the
203 same spots without the MP, i.e., the background illumination in water only. Such bright spots (shown
204 by red arrows in Fig. 1d correspond to "lensing effect" due to a very thin portion of the MP from
205 these smaller irregular areas the MP that focus incident light. Such an effect can exist only if the front
206 and back of a part of the MP is optically smooth. This property is hardly present with organic particles.
207 The lensing effect is therefore an additional feature for the discrimination of MP against other
208 particles.

209 There are other less bright yellowish spots showing transparency or translucency, but darker areas
210 dominate over the whole MP surface in Fig. 1d that are due to light scattering and complex shape of
211 this MP. A narrow dark bridge is located in the bottom part of the MP, and it encloses a relatively
212 large bright area that is actually water (shown by the black arrow in Fig. 1d), i.e., a hole in the MP.
213 This MP is relatively large, and phenomena of geometrical optics apply for light interaction with the
214 MP. Obtaining MPs with very complex shape is one advantage of the grinding method used to
215 generate them. It creates MPs similar to the ones formed in natural environment with no predefined
216 shape, unlike other means, such as cutting leading to MP with high geometrical shapes, see Fig. 1e.

217 Fig. 1f is the description of the entire procedure allowing the imaging and recognition of MP particles
218 in a water sample using the commercial device.

219 Fig. 2 shows images of MPs obtained from originally transparent pristine plastics (PS and UPVC)
220 that have undergone similar preparation process as the translucent ones. Fig. 2a shows the image
221 (false color) for PS MP. Obviously, these scatter light like the MPs from the translucent MPs resulting
222 in a dark appearance in the image. Unlike in the previous samples, here, the grinding process of the
223 plastic sheet is the main reason for scattering of the incident light from roughened surface and possibly
224 also a volume inhomogeneity of the MPs. On the contrary, the MP obtained from UPVC, in Fig. 2b

(false color), shows a platy form with rather high transparency close to the middle. This large particle is enlarged in Figs. 2c and d for closer examination. Its edges appear darker since light rays are reflected and refracted and do not reach the detector. The contour of the MP (Fig. 2d) shows that UPVC particle is an irregular and truncated pyramid-like block.

From images acquired by the ultra-high definition analyzer, one can easily isolate MP particle and perform different analyses on the extracted image. The process is shown in Fig. 3 for the case of LDPE sample. Fig. 3b is an isolated MP obtained by simply cropping the central part of the original image (Fig. 3a) and removing the background (Fig. 3c). The image of the particle (the large LDPE MP highlighted by a red rectangle in Fig. 1c is a projection onto a plane and allow to estimate the surface area of the considered MP by counting the number of black pixels (Fig. 3d). One can remark that for high change in shape within the depth direction, such a data processing has a low significance, and an estimation of the volume would be more relevant. However, for tiny particle as in most of other presented cases, such a fast study, easily integrable into the software of the measurement device, gives a realistic evaluation of the shape and size of the plastic particles.

Similar processing and image projection was applied to PA, PP, and LDPE MPs and are summarized in Table 1. Concerning the number of particles, we counted the same amount (around 25) of MPs made of PP, PS, and LDPE in the 0.5 L of water. We counted about twice less (10) for the MP made of PA and only 3 particles for UPVC. These values are given only for illustration since the samples were homemade and the amount of MP/L is not known. The main aim of this study was to demonstrate the feasibility of imaging MP analysis by imaging them in tap water samples. The number of counted particles is different in each sample because the value comes from the analysis of one snapshot at a fixed time. However, such a figure indicates the possibilities offered by such a technique in examining a relatively large volume of water. It is to be noted that the analysis of larger sample volumes is also possible by using a continuous flow mode. Recognition of plastic particles can be implemented directly in the software through machine learning processes to automate the detection and counting process.

The shape of the MPs depends primarily on the plastic type. It is clear from Table 1 that MP from PP and PA are quite similar in shape whereas the ones from UPVC, PS, and LDPE are completely different. PS particles are more rounded than UPVC ones that are presenting clear facets and angles. LDPE MPs are the one presenting the most random shape including fibers, as shown in Fig. 4, apertures, and lens-type areas. The overall size distribution is relatively different also from a plastic type to another. For instance, LDPE present both large and small MP types. PA MPs have areas around 0.2 $mm^2$, which corresponds to the grinding tool while PP MPs are about twice smaller. It is

to be noted that the projection area of particles is more descriptive but exact quantity would be the volume of the MP which is not easy to access. This analysis can be used to anchored in the memory of the measurement device the characteristic shapes of the different MPs and help the teaching necessary for machine learning-based recognition.

Next, we consider the concept of light intensity bitmap analysis in more details. Although many MPs illustrated in this study have a dark appearance, they actually transmit light. This is a property that can be used in screening of MPs from wood fibers, human hair (quite often present in waste waters) and air bubbles. We start with the concept of light intensity ratio (M). It is defined as the ratio of the intensity of the transmitted light through an object in water to the intensity of light through water only (background). This ratio depends usually on the location of image pixel over the object. We have observed that a quantity 1 – M map is sensitive to screen between different objects in laminar water flow system.

Before demonstrating the full power of 1 – M map, we wish to remark that human hair and wood fibers (soft or hard) differ very much from the optical properties of a MP. Indeed, wood fibers have complex optical properties because it consists mostly of cellulose (refractive index ca. 1.53, crystalline cellulose is birefringent), hemicellulose (ca. 1.53) and lignin (ca. 1.61) [31], hence wood fibers present volume light scattering. Similarly, human hair can be considered as an organic material that has refractive index ca. 1.54.

In Fig. 5 is the 1 – M map of one snapshot captured by the high-resolution imaging device. By arrows, we highlight a human hair, a PP MP, a wood fiber with a kink and an air bubble captured in the image. The hair was introduced in sample of PP MPs and the wood fiber is due to previous measurement of wood pulp sample in the device. These four particles are analyzed in detail in Fig. 6.

On the left hand-side are shown the 1 – M maps, in the middle and on the right hand-side panels are 1 – M values taken from the locations shown by the colored arrows and lines on the 1 – M maps. It is also to be noted that representing 1 – M in figures allows a better contrast, but the discussion is done directly on the M-values. In the case of human hair, Fig. 6 a, M is oscillating along the length of the hair, with a mean value $\overline{\mathrm{M}} \simeq 0.7$ and a standard deviation $\sigma \simeq 0.1$. This oscillation in intensity is due to light interference. On the contrary, M varies a lot obtained in the cross-direction but has rather regular bell-shaped function following the shape of the hair itself. In Fig. 6 b is shown 1 – M for a soft wood fiber. In the location of the fiber between the two blue arrows M is fluctuating in an irregular manner and relatively big difference appear in the magnitude of the M ($\overline{\mathrm{M}} \simeq 0.6$ and $\sigma \simeq 0.08$). In the cross direction the M is changing strongly, and the distribution is not regular like in the

case of the human hair. The next case, Fig. 6c is the PP MP. Both in *x*- and *y*- directions 1 – M has pretty much a constant value ($\bar{M} \simeq 0.9$ and $\sigma \simeq 1.5 \cdot 10^{-4}$) different from the cases of wood fiber and human hair. In the inset are shown 1 – M for zoomed portions of this MP. Finally, in Fig. 6d, are 1 – M data for an air bubble ($\bar{M} > 0.9$ and $\sigma \simeq 1 \cdot 10^{-5}$). The data of air bubble show higher symmetry and regularity than the MP. Surely the circular appearance of air bubble discriminates it from this MP. However, one might think that a spherical primary MP could be mixed with an air bubble. However, optical properties of an air bubble and primary spherical MPs are quite different. Firstly, the refractive index ratio of water- air bubble is much higher than that of water -primary spherical MP which has consequences both in light reflection and refraction in such objects. Furthermore, a flowing air bubble may not be perfect sphere but can be flattened. Detection of primary MPs is a topic of our future studies. This is enabled by the refractive index difference between the media leading to variations in the light intensity bitmap.

In the case of a mixture of different plastic type MPs in water their presence can be revealed by the light intensity map, but their specific plastic type cannot be identified. We think this sorting of different MPs directly from water is at least a partial solution to avoid laborious laboratory studies and would be a practical concept to investigate industrial and urban wastewaters taken, e.g., from onsite pipelines. The device is portable and either single or double devices could be used before a filter to pre-screen any presence of MPs and their images and characterization like done above, and after the filter to monitor again presence of possible remaining MPs in water.

## 4. Discussion

This study reports on imaging of homemade MPs that have irregular shapes and structures. Irregular MPs, such as fragments, are found in aquatic environments. Typical properties of interest of MPs are their size, shape, abundance, and the type of plastic [32]. This information can be obtained by using a several imaging techniques based on microscopies namely light, fluorescent, polarization, scanning or transmission electron, atomic force microscopies [8,33], and hyperspectral imaging [34]. However, these conventional devices require extensive pretreatment methods and are also time consuming as well as limitation imposed the resolution of some of these devices. In most cases, visual inspection, with it challenges, may precede these methods. For sorting of MPs from other materials, the commercial imaging device is showing promising features for pre-screening of MPs directly from a water sample. However, the data are not obtained continuously as a function of time because the recorded video consists of image frames after snapshot illumination. Hence, there is a deadtime

between successive illumination and image capturing, and MPs can be flow pass without detection. Nevertheless, each image frame can be studied later, like in this paper for observation of MPs and their abundance. Such an abundance gives minimum estimate of MPs in a water sample. This would give statistical results useful in industry, for instance. Improved data processing can be implemented directly in the device's software and combined with automatic recognition of plastics particles. This last step requires machine learning process to teach the device since plastics have some characteristic shape, size, and optical features to be compared to other organic or inorganic particles.

The light intensity ratio is suggested as a measure to screen presence of a MP by using the regularity of 1 – M obtained over a MP. Hence, it serves as a parameter that a MP has been found but it cannot identify the plastic type. This finding of a MP is already important step regarding the laborious current procedures in laboratories. Extensive identification of MPs would require measurement of spectral properties from MPs, but there is currently no such measurement mode in the device. However, this can be integrated in future. Alternatively, one can attach other modes to filter the measured water volume to detect dry MPs using, e.g., portable reflectometer [35] or Raman spectrometer [36] from a mixture of MPs. This would make identification of MPs possible in field conditions such as municipal or industrial wastewater treatment plants. In addition, reliable and fast methods for MP analysis are urgently needed for environmental monitoring. Driving forces include, e.g., international agreements or policies such as EU Marine Strategy Framework Directive [37]. Currently, samples for monitoring MPs are collected infrequently and results are obtained after laborious analysis in research laboratories, and thus, relatively fast on-site analysis would be appreciated. Using demonstrated imaging methods during a research cruise, large-scale monitoring campaigns would reveal local and temporal changes rather than indicate only the abundance of MPs.

The results presented here based on UHD imaging brings the goal of field measurements of MPs directly from water samples nearer. After further development, imaging methods for MP analysis may be rather easily integrated to industrial process water or wastewater monitoring, because similar techniques are already used, e.g., for fiber analysis. This requires further development of spectral measurements to identify the MPs as well as image processing, e.g., to estimate real projection area of a MP as we have demonstrated by bitmap study of present samples. Image data from MPs show that it is possible to screen between transparent and translucent MPs.

The intensity ratio M, and therefore 1 – M, varies significantly with the refractive index of the particle and its overall optical properties. We also showed that these values can vary along preferential directions with a relatively high contrast (proportional to the standard deviation of M) but with a quite high mean value, this is the case of a hair. M values can be randomly fluctuating showing low mean

value and similar standard deviation than the hair, this is the case of a wood fiber. M values can be very high and nearly constant for an air bubble. Finally, for a microplastic, M present high values, still lower that for an air bubble and wood fiber, with low but not negligible fluctuations. Combining conclusions on the statistics of M values and their distribution on several key-directions of the particles, is a clear indicator of the particle type.

In case of a biofilm attached over MP it is usually an issue and typically requires removal in sample preparation prior to MP characterization. In case of transparent biofilm, that consists mostly of water, identification of MP by 1 – M should not be problematic, but this requires further experiments. In case of a heterogenous opaque biofilm there are more challenges but the intensity ratio, if non- zero, is a convolution of transmittance of MP and the biofilm. This too requires future experiments in trying to identification of a MP beneath the opaque biofilm.

## 5. Conclusion

We demonstrate in this research that a commercially available image analyzer primarily designed for the detection of wood fibers in aquatic samples can be efficiently used for MP detection. Using this device, we have been able to determine the shape, size (projected surface), analyzed microplastics prepared by grinding of five common plastic sheets namely, PA, PP, LDPE, PS, and UPVC. The results show that the microplastics exhibit clear difference in terms of shapes and transparency, after grinding, which arise from the mechanical properties of the plastic type and can, therefore, be used as an indirect way to classify plastic types. The size of the particles differs also from one plastic to another, despite using the same settings for the grinding tool. Combining the ultra-high-definition imaging along with the light bitmap obtained from the device with automated machine learning would lead to a complete device for MP recognition in wastewater treatment environment as the device can already distinguish MPs, wood fibers, human hair, and air bubbles.

## Acknowledgements

We acknowledge the financial support of the Academy of Finland through the flagship on “Photonics research and innovation” (PREIN, 320166) and of Business Finland through the project on “Circulating economy of water in industrial processes” (CEIWA, #541/31/2021).

## FIGURES AND TABLES

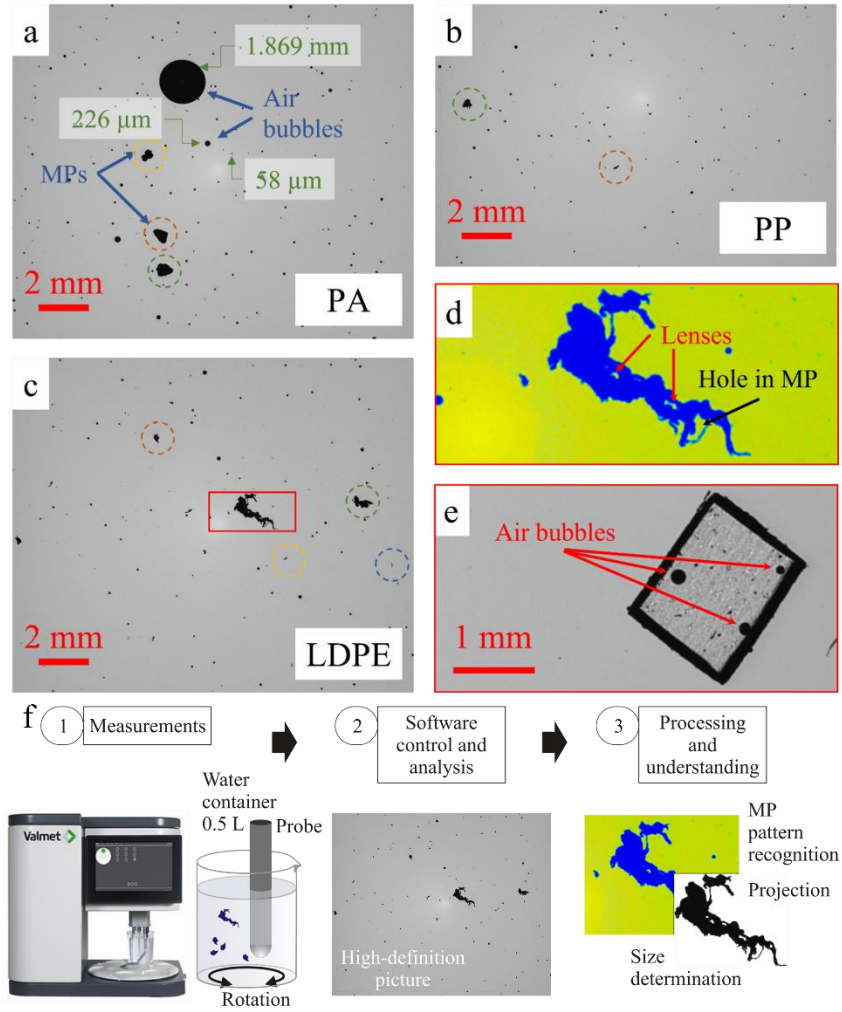


*Figure 1: Images acquired with Valmet FS5 UHD device for different samples in water including a) PA particles, b) PP particles, and c) LDPE particles. d) zoomed-in and enhanced image of a microplastic particle from c) (red contour). Red arrows in d) highlight bright "lensing" areas in the microplastic particle. Black arrows in d) highlights a hole in the MP. e) air bubbles on a PET MP. f) Procedure to image and recognize MPs in a water sample.*

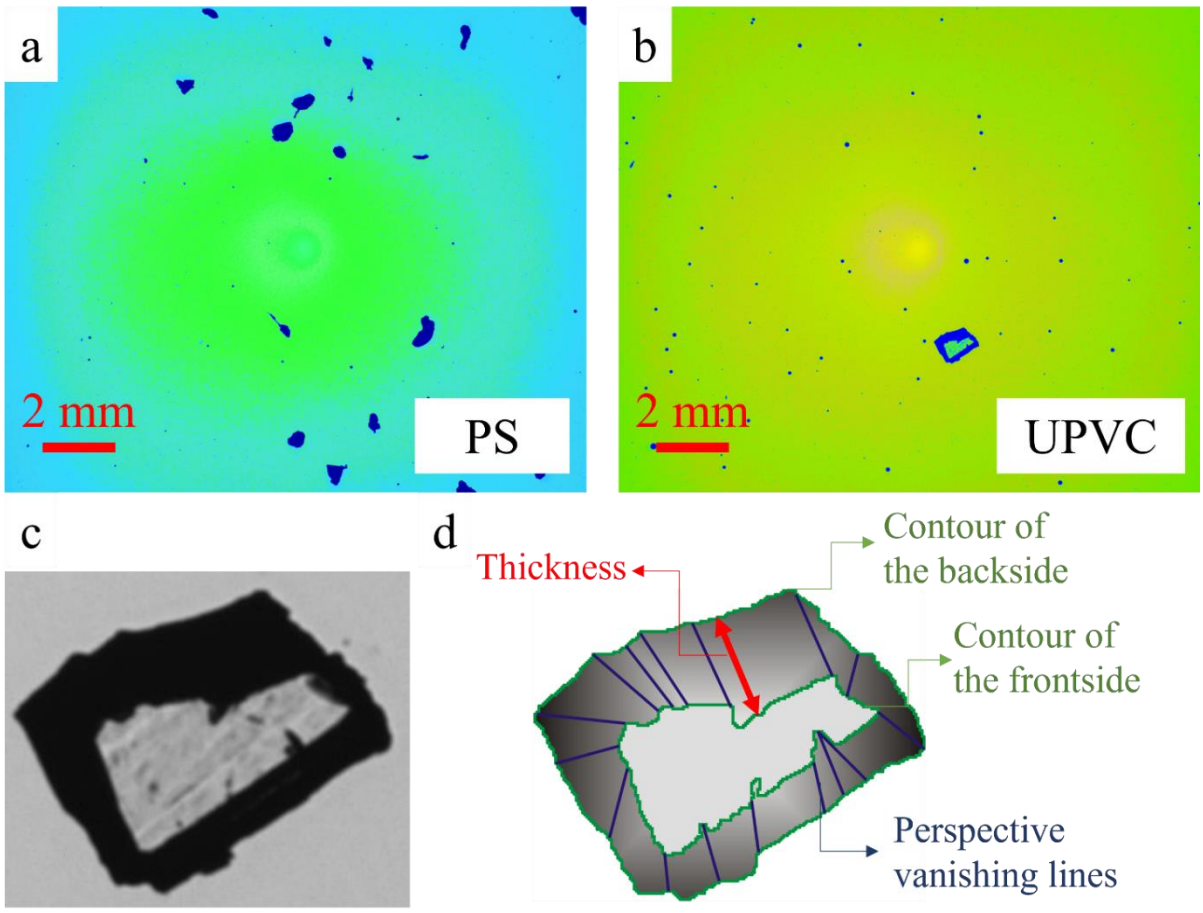


*Figure 2: Processed images in order to highlight the different plastic microparticles a) PS and b) UPVC plastic particles. Highlight on UPVC particle: c) Original cropped image and d) contoured image showing an irregular-cut pyramid due to the grinding.*

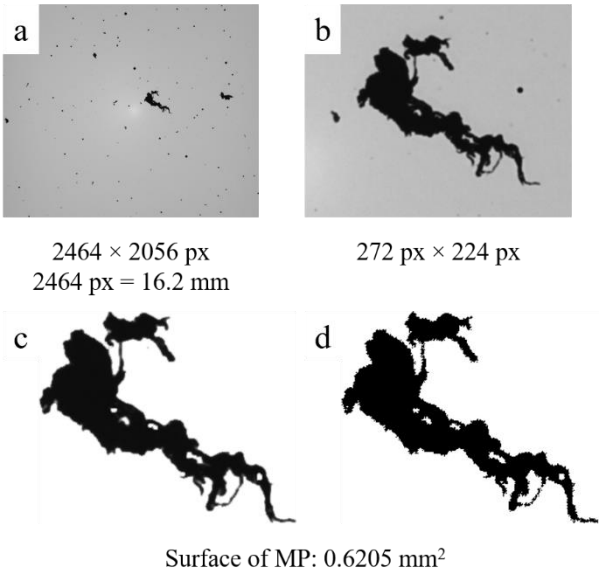


403

404 *Figure 3: Isolating MP from the acquired images and extracting an estimation of the projected*
405 *surface area of the particle. a) original image, b) cropped image, c) isolated MP, and d) projected*
406 *image of the MP in black and white allowing an estimation of the size.*

407

408

409

410

411 *Table 1: Selected MP extracted from Fig. 1 to estimate the surface area: Plastic types and*
412 *corresponding figures from which the MP images have been extracted; isolated MPs without*
413 *background; projected images for pixels counting; surface area of the MP.*

| Plastic type / color of the dashed circle on Fig. 2a | Isolated image of MPs | Projected image | Surface area of the MP [$mm^2$] |
|---|---|---|---|
| PA / Green<br>in Fig. 2a |  |  | 0.252 |
| PA / Brown<br>in Fig. 2a |  |  | 0.219 |
| PA / Yellow<br>in Fig. 2a |  |  | 0.134 |
| PP / Green<br>in Fig. 2b |  |  | 0.092 |
| PP / Brown<br>in Fig. 2b |  |  | 0.016 |
| LDPE / Red rectangle<br>in Fig. 2c / Fig. 2d |  |  | 0.621 |
| LDPE / Yellow<br>in Fig. 2c |  |  | 0.007 |

| | | | |
|---|---|---|---|
| LDPE / Blue<br>in Fig. 2c |  |  | 0.004 |
| LDPE / Green<br>in Fig. 2c |  |  | 0.176 |
| LDPE / Brown<br>in Fig. 2c |  |  | 0.048 |

414

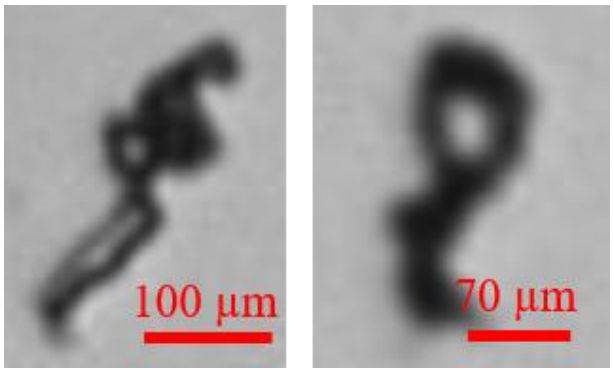


*Figure 4: Image of MP extracted from Fig. 2c (LDPE samples) showing opening, facets, or "lenses" in the particles.*

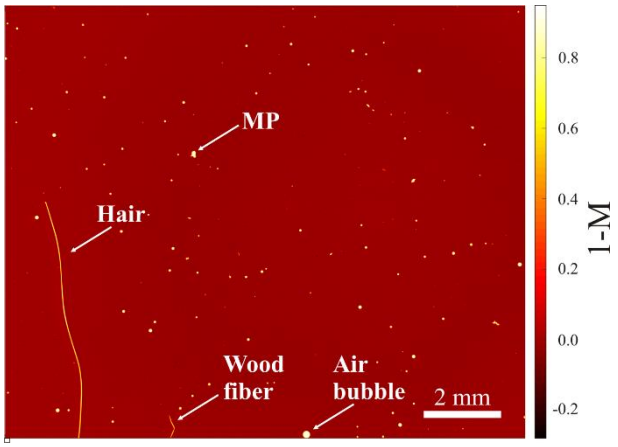


*Figure 5: Example of a 1 – M map obtained from one snapshot captured by UHD FS5 device. It shows a human hair, a kinked soft wood fiber, a PP microplastic and an air bubble. Each particle is further analyzed in Fig. 6.*

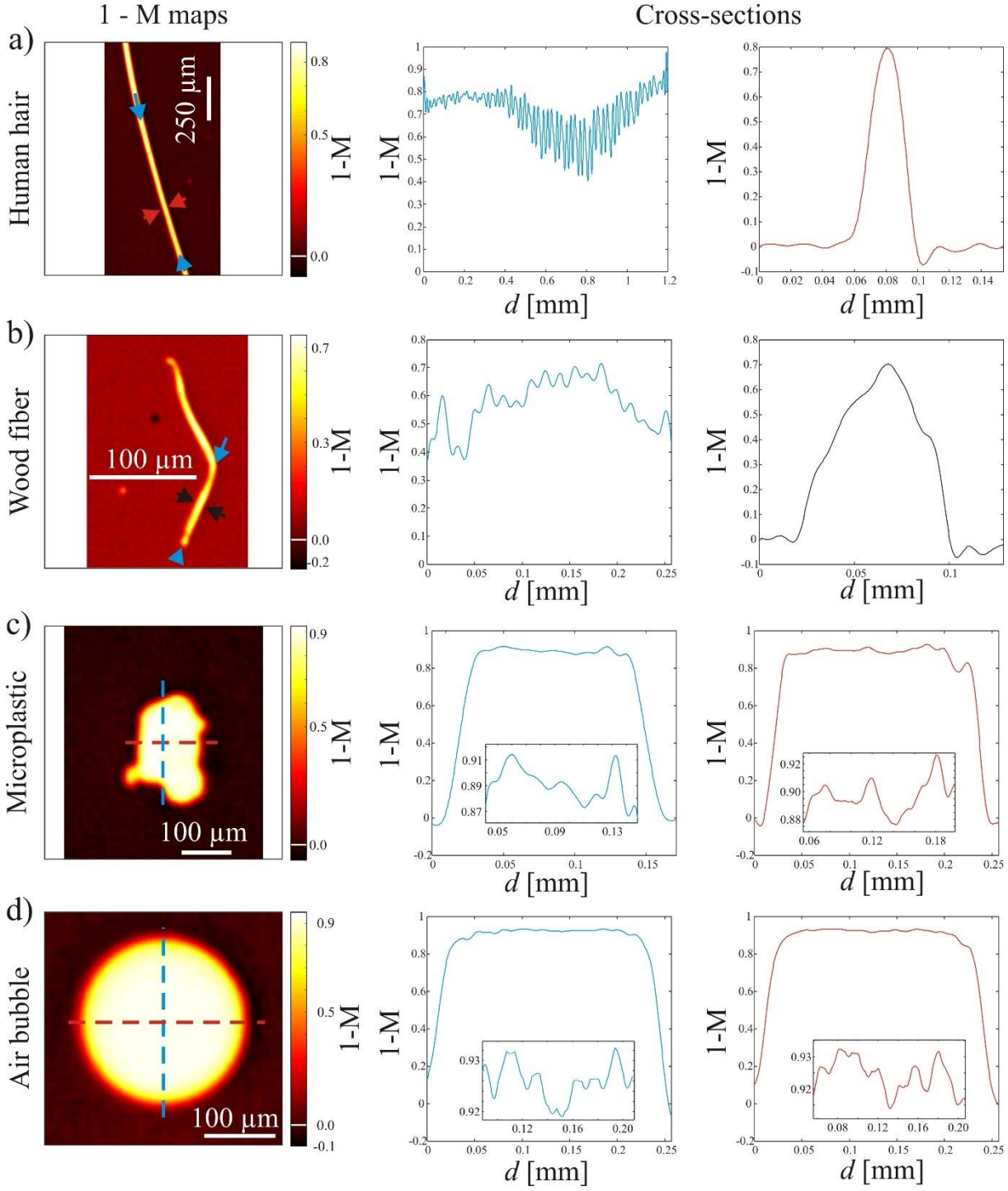


*Figure 6: Intensity distribution analysis through 1 – M values for a) a human hair, b) a soft wood fiber, c) a microplastic, and d) an air bubble. Left: 1 – M maps. Middle and right: cross-section along the colored arrows or dashed lines shown on the 1 – M maps. Insets in c) and d) are zoom-in curves on the central part of the 1 – M cross-sections.*

## References


1. Campanale, C., Massarelli, C., Savino, I., Locaputo, V., Uricchio, V.F., 2020. A detailed review study on potential effects of microplastics and additives of concern on human health. Int. J. Environ. Res. Public Health 17. https://doi.org/10.3390/ijerph17041212
2. Peixoto, D., Pinheiro, C., Amorim, J., Oliva-Teles, L., Guilhermino, L., Vieira, M.N., 2019. Microplastic pollution in commercial salt for human consumption: A review. Estuar. Coast. Shelf Sci. 219, 161–168. https://doi.org/10.1016/j.ecss.2019.02.018
3. Wanner, P., 2021. Plastic in agricultural soils – A global risk for groundwater systems and drinking water supplies? – A review. Chemosphere 264, 128453. https://doi.org/10.1016/j.chemosphere.2020.128453
4. Asamoah, B.O., Uurasjärvi, E., Räty, J., Koistinen, A., Roussey, M., Peiponen, K., 2021. Towards the Development of Portable and In Situ Optical Devices for Detection of Micro- and Nanoplastics in Water : A Review on the Current Status. Polym. Eng. Sci. 13, 730. https://doi.org/https://doi.org/10.3390/polym13050730
5. Becucci, M., Mancini, M., Campo, R., Paris, E., 2022. Microplastics in the Florence wastewater treatment plant studied by a continuous sampling method and Raman spectroscopy : A preliminary investigation. Sci. Total Environ. 808, 152025. https://doi.org/10.1016/j.scitotenv.2021.152025
6. Elsayed, A.A., Erfan, M., Sabry, Y.M., Dris, R., Gaspéri, J., Barbier, J.S., Marty, F., Bouanis, F., Luo, S., 2021. A microfluidic chip enables fast analysis of water microplastics by optical spectroscopy. Sci. Rep. 1–11. https://doi.org/10.1038/s41598-021-89960-4
7. Faltynkova, A., Johnsen, G, WAGNER, M., 2021. Hyperspectral imaging as an emerging tool to analyse microplastics: A systematic review and recommendation for future development, Microplastics and Nanoplastics, 1, 13.
8. Mariano, S., Tacconi, S., Fidaleo, M., Rossi, M., Dini, L., 2021. Micro and Nanoplastics Identification: Classic Methods and Innovative Detection Techniques. Front. Toxicol. 3, 1–17. https://doi.org/10.3389/ftox.2021.636640
9. Behal, J., Valentino, M., Miccio, L., Bianco, V., Itri, S., Mossotti, R., Dalla Fontana, G., Stella, E., Ferraro, P., 2022. Toward an all-optical fingerprint of syntetic and natural microplastic fibers by polarization-sensitive holographic microscopy, ACS Photonics, 9, 694-705.
10. Asamoah, B.O., Kanyathare, B., Roussey, M., Peiponen, K.-E., 2019. A prototype of a portable optical sensor for the detection of transparent and translucent microplastics in

freshwater. Chemosphere 231. https://doi.org/10.1016/j.chemosphere.2019.05.114

11. Leonard, J., Koydemir, H., Koutnik, H. C., Tseng, V. S., Oscan A., Mohanty, S. K., 2022, Smart-phone enabled rapid quantification of microplastics, J. Haz. Mat. Lett., 3, 10052.
12. Haapala, A., Laitinen, O., Karinkanta, P., Liimatainen, H., 2013. Optical characterisation of size, shape and fibrillarity from microfibrillar and microcrystalline cellulose, and fine ground wood powder fractions. Appita J. 66, 331–339.
13. Valentino, M., Jaromír, B., Bianco, V., Itri, S., Mossotti, R., Dalla, G., Battistini, T., Stella, E., Miccio, L., Ferraro, P., 2022. Intelligent polarization-sensitive holographic fl ow-cytometer : Towards speci fi city in classifying natural and microplastic fi bers. Sci. Total Environ. 815. https://doi.org/10.1016/j.scitotenv.2021.152708
14. Peiponen, K.-E., Jukka, R., Ishaq, U., Pélisset, S., Ali, R., 2019. Outlook on optical identification of micro- and nanoplastics in aquatic environments. Chemosphere 214, 424–429. https://doi.org/10.1016/j.chemosphere.2018.09.111
15. Abaroa-Perez, B., Ortiz-Montoa, S., Hernandez-Brito, J. J, Vega-Moreno, D., 2022, Yellowing, weathering and degradation of marine pellets and their influence on the adsorption of chemical pollutants, Polymers (Basel), 14, 1303.
16. Lv, L., Yan, X., Feng, L., Jiang, S., Lu, Z., Xie, H., Sun, S., Chen, J., Li, C., 2021. Challenge for the detection of microplastics in the environment 2010, 5–15. https://doi.org/10.1002/wer.1281
17. Morét-ferguson, S., Lavender, K., Proskurowski, G., Murphy, E.K., Peacock, E.E., Reddy, C.M., 2010. The size , mass , and composition of plastic debris in the western North Atlantic Ocean 60, 1873–1878. https://doi.org/10.1016/j.marpolbul.2010.07.020
18. Zhao, S., Danley, M., Ward, J.E., Mincer, T.J., 2017. An approach for extraction, characterization and quantification of microplastics in marine snow using Raman microscopy. Anal. Methods 9, 1470–1478. https://doi.org/10.1039/c6ay02302a
19. Löder, M.G.J., Gerdts, G., 2015. Methodology Used for the Detection and Identification of Microplastics—A Critical Appraisal, in: Bergmann, M., Gutow, L., Klages, M. (Eds.), Marine Anthropogenic Litter. Springer Open, p. 214.
20. Haapala, A., Levanic, J., Nadrah, P., 2020. Analyzing TEMPO-Oxidized Cellulose Fiber Morphology: New Insights into Optimization of the Oxidation Process and Nanocellulose Dispersion Quality˅. https://doi.org/10.1021/acssuschemeng.0c05989
21. Kanyathare, B., Asamoah, B. O., Ishaq, U., Amoani, J., Räty, J., Peiponen, K.-E., 2020. Optical transmission spectra study in visible and near-infrared spectral range for identification of rough transparent plastics in aquatic environment, Chemosphere, 248, 126071.

22. Doyle, M.J., Watson, W., Bowlin, N.M., Sheavly, S.B., 2011. Plastic particles in coastal pelagic ecosystems of the Northeast Paci fi c ocean. Mar. Environ. Res. 71, 41–52. https://doi.org/10.1016/j.marenvres.2010.10.001
23. Piarulli, S., Sciutto, G., Oliveri, P., Malegori, C., Prati, S., Mazzeo, R., Airoldi, L., 2020. Rapid and direct detection of small microplastics in aquatic samples by a new near infrared hyperspectral imaging (NIR-HSI) method. Chemosphere 260, 127655. https://doi.org/10.1016/j.chemosphere.2020.127655
24. Huang, H., Ullah, J., Shuchang, Q., Zehao, L., Chunfang, S., Wang, H., 2020. Hyperspectral Imaging as a Potential Online Detection Method of Microplastics. Bull. Environ. Contam. Toxicol. https://doi.org/10.1007/s00128-020-02902-0
25. Bianco, V., Memmolo, P., Cargani, P., Merola, F., Paturzo, M., Distarte, C., Ferraro, P., 2020, Adv. Intell. Syst., 2, 1900153.
26. Horisaki, R., Fujii, K., Tanida, J., 2018. Single-shot and lensless complex-amplitude imaging with incoherent light based on machine learning. Opt. Rev., 25, 593-597.
27. Selmke, M., 2020. Bubble optics. Appl. Opt. 59, 45–58.
28. Senouci-Bereksi, M., Kies, F.K., Bentahar, F., 2018. Hydrodynamics and Bubble Size Distribution in a Stirred Reactor. Arab. J. Sci. Eng. 43, 5905–5917. https://doi.org/10.1007/s13369-018-3071-z
29. Walls, P.L.L., Bird, J.C., Bourouiba, L., 2014. Moving with bubbles: a review of the interactions between bubbles and the microorganisms that surround them. Integr. Comp. Biol. 54, 1014–1025. https://doi.org/10.1093/icb/icu100
30. Renner, G., Nellessen, A., Schwiess, A., Wenzel, M., Schmidt, T. C., Schram J., 2020. Hydrophobicity - water/air based enrichment cell for microplastics analysis within environmental samples: A proof of concept, Methods X 7, 100732.
31. Li, Y., Fu, Q., Yu, S., Yan, M., Berglund, L., 2016. Optically transparent wood from a nanoporous cellulosic template, Biomacromolecules 17, 1358 -1364.
32. Enders, K., Lenz, R., Stedmon, C.A., Nielsen, T.G., 2015. Abundance, size and polymer composition of marine microplastics ≥10 μm in the Atlantic Ocean and their modelled vertical distribution. Mar. Pollut. Bull. 100, 70–81. https://doi.org/10.1016/j.marpolbul.2015.09.027
33. Woo, H., Seo, K., Choi, Y., Kim, J., Tanaka, M., Lee, K., Choi, J., 2021. Methods of Analyzing Microsized Plastics in the Environment. Appl Sci 11, 10640.
34. Zhao, J., Liu, L., Zhang, Y., Wang, X., Wu, F., 2018. A novel way to rapidly monitor microplastics in soil by hyperspectral imaging technology and chemometrics. Environ. Pollut. 238, 121–129. https://doi.org/10.1016/j.envpol.2018.03.026

35. Feather, J.W., Ellis, D.J., Leslie, G., 1988. A portable reflectometer for the rapid quantification of cutaneous haemoglobin and melanin. Phys. Med. Biol. 33, 711–722.
36. Crocombe, R.A., 2018. Portable Spectroscopy. Appl. Spectrosc. 72, 1701–1751. https://doi.org/10.1177/0003702818809719
37. European Union, 2008. DIRECTIVE 2008/56/EC OF THE EUROPEAN PARLIAMENT AND OF THE COUNCIL of 17 June 2008 establishing a framework for community action in the field of marine environmental policy (Marine Strategy Framework Directive), Official Journal of the European Union.